

Gravitational waves from the sound of a first order phase transition

Mark Hindmarsh,^{1,2,*} Stephan J. Huber,^{1,†} Kari Rummukainen,^{2,‡} and David J. Weir,^{2,§}

¹ *Department of Physics and Astronomy, University of Sussex, Falmer, Brighton BN1 9QH, U.K.*

² *Department of Physics and Helsinki Institute of Physics, PL 64*

(Gustaf Hällströmin katu 2), FI-00014 University of Helsinki, Finland

(Dated: April 9, 2013)

We report on the first 3-dimensional numerical simulations of first-order phase transitions in the early universe to include the cosmic fluid as well as the scalar field order parameter. We calculate the gravitational wave (GW) spectrum resulting from the nucleation, expansion and collision of bubbles of the low-temperature phase, paying particular attention to those sourced by the fluid. We find that the fluid continues to be a source of GWs long after the bubbles have merged, a new effect not taken into account in previous modelling of the GW source based on the envelope approximation. The kinetic energy of the fluid is in the form of compression waves: the main source of the GWs after a phase transition is therefore the sound the bubbles make.

PACS numbers: 64.60.Q-, 47.75.+f, 95.30.Lz

In a hot Big Bang there were phase transitions in the early Universe [1, 2], which may well have been of first order; one major consequence of such a transition would be the generation of gravitational waves [3–8]. The electroweak transition in the Standard Model is known to be a cross-over [9–11] but it may be first order in minimal extensions of the Standard Model [12–17]. It is therefore essential to properly characterise the expected power spectrum from first-order phase transitions.

First order phase transitions proceed by the nucleation, growth, and merger of bubbles of the low temperature phase [3, 18–25]. The collision of the bubbles is a violent process, and both the scalar order parameter and the fluid of light particles generate gravitational waves.

Numerical studies have been carried out of the behaviour of bubbles in such a phase transition using spherically symmetric (1+1)-dimensional simulations [23, 24]. The calculation of the gravitational wave spectrum has been refined in the intervening years using the semi-analytic envelope approximation [5, 7, 8, 26–28]. Fully 3D simulations of the scalar field only have been carried out [29], qualitatively supporting the envelope approximation, and pointing out important gravitational wave production from the scalar field after the bubble merger.

In a hot phase transition, the fluid plays an important role, firstly as a brake on the scalar field, and secondly as a source of gravitational waves itself. The fluid has generally been assumed to be incompressible and turbulent [30–33]. An important question for the gravitational wave power spectrum is the validity of this modelling, which generally borrows from the Kolmogorov theory of non-relativistic driven incompressible turbulence.

In this Letter we report on the first fully three dimensional simulation of bubble nucleation involving a coupled field-fluid system. We make use of these simulations to calculate the power spectrum of gravitational radiation from a first-order phase transition. We find that the compression waves in the fluid – sound waves – continue

to be an important source of gravitational waves for up to a Hubble time after the bubble merger has completed. This boosts the signal by the ratio of the Hubble time to the transition time, which can be orders of magnitude.

The system describing the matter in the early universe consists of a relativistic fluid coupled to a scalar field, which acquires an effective potential

$$V(\phi, T) = \frac{1}{2}\gamma(T^2 - T_0^2)\phi^2 - \frac{1}{3}\alpha T\phi^3 + \frac{1}{4}\lambda\phi^4. \quad (1)$$

The rest-frame pressure p and energy density ϵ are

$$\epsilon = 3aT^4 + V(\phi, T) - T\frac{\partial V}{\partial T} \quad (2)$$

$$p = aT^4 - V(\phi, T) \quad (3)$$

with $a = (\pi^2/90)g$, and g the effective number of relativistic degrees of freedom contributing to the pressure at temperature T . The stress-energy tensor for a scalar field ϕ and an ideal relativistic fluid U^μ is

$$T^{\mu\nu} = \partial^\mu\phi\partial^\nu\phi - g^{\mu\nu}[\frac{1}{2}\partial_\alpha\phi\partial^\alpha\phi] + [\epsilon + p]U^\mu U^\nu + g^{\mu\nu}p \quad (4)$$

where the metric convention is $(-+++)$. The scalar field potential is included in the definition of p . We split $\partial_\mu T^{\mu\nu} = 0$ (nonuniquely) into field and fluid parts with a dissipative term permitting transfer of energy between the scalar field and the fluid $\delta^\nu = \eta U^\mu \partial_\mu \phi \partial^\nu \phi$ [23].

Given these expressions, the equations of motion can be derived. For the field we have

$$-\ddot{\phi} + \nabla^2\phi - \frac{\partial V}{\partial\phi} = \eta W(\dot{\phi} + V^i\partial_i\phi) \quad (5)$$

where W is the relativistic γ -factor and V^i is the fluid 3-velocity, $U^i = WV^i$. For the fluid energy density $E = W\epsilon$, contracting $[\partial_\mu T^{\mu\nu}]_{\text{fluid}}$ with U_ν yields

$$\begin{aligned} \dot{E} + \partial_i(EV^i) + p[\dot{W} + \partial_i(WV^i)] - \frac{\partial V}{\partial\phi}W(\dot{\phi} + V^i\partial_i\phi) \\ = \eta W^2(\dot{\phi} + V^i\partial_i\phi)^2. \end{aligned} \quad (6)$$

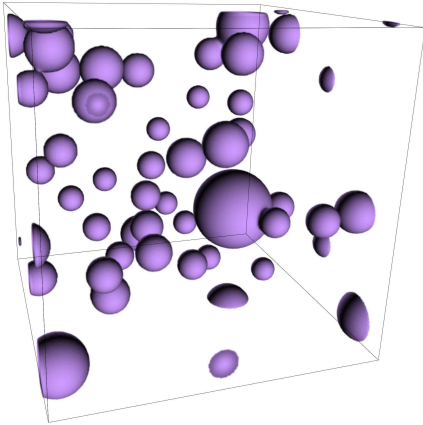


FIG. 1: Snapshot of scalar field ϕ at $t = 400 T_c^{-1}$, for $\eta = 0.2$ with the ‘weak’ transition parameters. Regions with $\phi < 1$ are transparent. See Fig. 2 for the energy density on a spatial slice at this timestep.

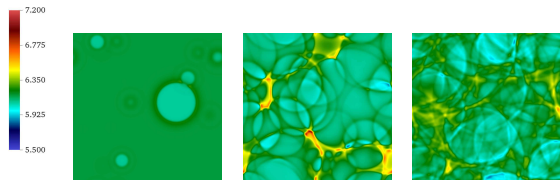


FIG. 2: Slices of fluid energy density E/T_c^4 at $t = 400 T_c^{-1}$, $t = 800 T_c^{-1}$ and $t = 1200 T_c^{-1}$ respectively, for the $\eta = 0.2$ simulation. The slices correspond roughly to the end of the nucleation phase, the end of the initial coalescence phase and the end of the simulation.

The equations of motion for the fluid momentum density $Z_i = W(\epsilon + p)U_i$ read

$$\dot{Z}_i + \partial_j (Z_i V^j) + \partial_i p + \frac{\partial V}{\partial \phi} \partial_i \phi = -\eta W(\dot{\phi} + V^j \partial_j \phi) \partial_i \phi. \quad (7)$$

The principal observable of interest to us is the power spectrum of gravitational radiation resulting from bubble collisions. To calculate this we use the procedure detailed in Ref. [34]. We evolve the *unprojected* equation of motion for the metric perturbations

$$\ddot{u}_{ij} - \nabla^2 u_{ij} = 16\pi G(\tau_{ij}^\phi + \tau_{ij}^f), \quad (8)$$

where $\tau_{ij}^\phi = \partial_i \phi \partial_j \phi$ and $\tau_{ij}^f = W^2(\epsilon + p)V_i V_j$. We recover the physical metric perturbations in momentum space $h_{ij}(\mathbf{k}) = \lambda_{ij,lm}(\hat{\mathbf{k}})u_{lm}(t, \mathbf{k})$, where $\lambda_{ij,lm}(\hat{\mathbf{k}})$ is the projector onto transverse, traceless symmetric rank 2 tensors. We are most interested in the metric perturbations sourced by the fluid, as the fluid shear stresses generally dominate over those of the scalar field, although it will be instructive to also consider both sources together.

Having obtained the metric perturbations, the power spectrum per logarithmic frequency interval is

$$\frac{d\rho_{\text{GW}}(k)}{d \ln k} = \frac{1}{32\pi G L^3} \frac{k^3}{(2\pi)^3} \int d\Omega \left| \dot{h}_{lm}(t, \mathbf{k}) \right|^2. \quad (9)$$

We simulate the system on a cubic lattice of $N^3 = 1024^3$ points, neglecting cosmic expansion which is slow compared with the transition rate. The fluid is implemented as a three dimensional relativistic fluid [35], with donor cell advection. The scalar and tensor fields are evolved using a leapfrog algorithm with a minimal stencil for the spatial Laplacian. Principally we used lattice spacing $\delta x = 1 T_c^{-1}$ and time step $\delta t = 0.1 T_c^{-1}$, where T_c is the critical temperature for the phase transition. We have checked the lattice spacing dependence by carrying out single bubble self-collision simulations for $L^3 = 256^3 T_c^{-3}$ at $\delta x = 0.5 T_c^{-1}$, for which the value of ρ_{GW} at $t = 2000 T_c^{-1}$ increased by 10%, while the final total fluid kinetic energy increased by 7%. Simulating with $\delta t = 0.2 T_c^{-1}$ resulted in changes of 0.3% and 0.2% to ρ_{GW} and the kinetic energy respectively.

Starting from a system completely in the symmetric phase, we model the phase transition by nucleating new bubbles according to the probability per unit volume and time $P = P_0 \exp(\beta(t - t_0))$. Having decided to nucleate in a suitable untouched region of the box, we insert a static bubble with a gaussian profile for the scalar field.

We first studied a system with $g = 34.25$, $\gamma = 1/18$, $\alpha = \sqrt{10}/72$, $T_0 = T_c/\sqrt{2}$ and $\lambda = 10/648$; this allows comparison with previous (1 + 1) and spherical studies of a coupled field-fluid system where the same parameter choices were used [23]. The transition in this case is relatively weak: in terms of α_T , the ratio between the latent heat and the total thermal energy, we have $\alpha_{T_N} = 0.012$ at the nucleation temperature $T_N = 0.86 T_c$. We therefore also performed simulations with $\gamma = 2/18$ and $\lambda = 5/648$, for which $\alpha_{T_N} = 0.10$ at the nucleation temperature $T_N = 0.8 T_c$, which we refer to as an intermediate strength transition.

For the nucleation process, we took $\beta = 0.0125 T_c$, $P_0 = 0.01$ and $t_0 = t_{\text{end}} = 2000 T_c^{-1}$. The simulation volume allowed the nucleation of 100-300 bubbles, corresponding to a mean spacing between bubbles of order $100 T_c^{-1}$. Although the wall velocity is captured correctly, there is not enough time for the bubble walls to fully relax to their invariant scaling profile before colliding. Typically, the peak velocity prior to collision is 20-30% below the scaling value for the deflagrations.

For the weak transition we chose $\eta = 0.1, 0.2, 0.4$ and 0.6 . The first gives a detonation with wall speed $v_w \simeq 0.71$, and the others weak deflagrations with $v_w \simeq 0.44, 0.24$, and 0.15 respectively. The shock profiles are found in Figs. 2 and 3 of Ref. [23]. The intermediate transition was simulated at $\eta = 0.4$, for which the wall speed is $v_w \simeq 0.44$, very close to the weak transition with $\eta = 0.2$.

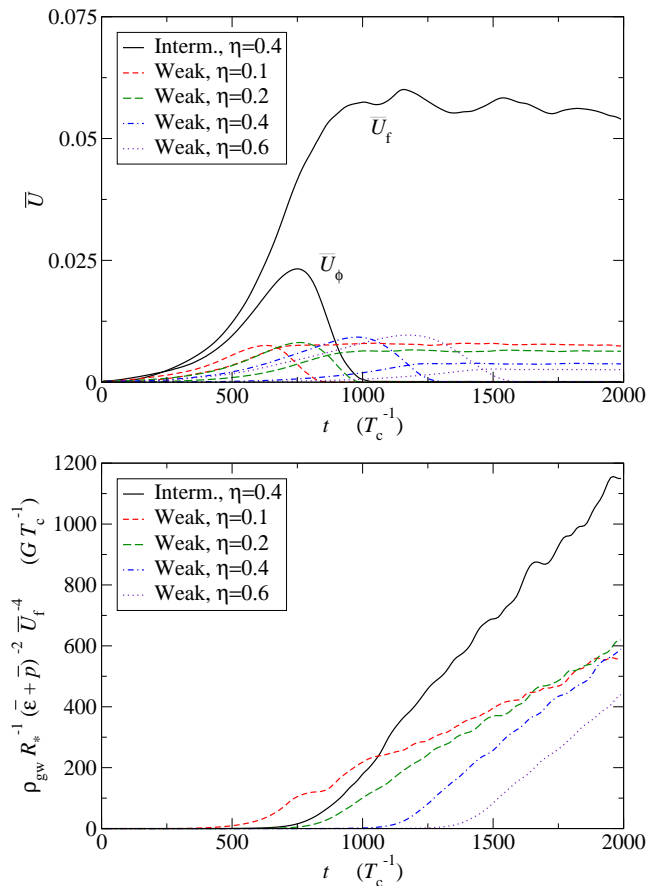


FIG. 3: Top: time series of \bar{U}_ϕ and \bar{U}_f (10), showing the progress of the phase transition; the curves for \bar{U}_ϕ and \bar{U}_f are individually identified for the ‘intermediate’ case. Bottom: time series of $\rho_{\text{GW}} R_*^{-1} (\bar{\epsilon} + \bar{p})^{-2} \bar{U}_f^{-4} (t_f)$, showing the evolution of the gravitational wave energy density relative to an estimate of the square of the final fluid shear stresses.

Fig. 3 (top) shows the time evolution of two quantities \bar{U}_ϕ and \bar{U}_f , defined so that

$$(\bar{\epsilon} + \bar{p}) \bar{U}_\phi^2 = \frac{1}{V} \int d^3x \tau_{ii}^\phi \quad \text{and} \quad (\bar{\epsilon} + \bar{p}) \bar{U}_f^2 = \frac{1}{V} \int d^3x \tau_{ii}^f \quad (10)$$

where $\bar{\epsilon}$ and \bar{p} are the volume-averaged rest-frame energy density and pressure respectively.

The squares of these quantities give an estimate of the size of the shear stresses of the field and the fluid relative to the background fluid enthalpy density, while \bar{U}_f tends to the r.m.s. fluid velocity for $\bar{U}_f \ll 1$. We see that \bar{U}_ϕ grows and decays with the total surface area of the bubbles of the new phase, while the mean fluid velocity grows with the volume of the bubbles, and then stays constant once the bubbles have merged. The slight decreasing trend in \bar{U}_f for the intermediate transition is a numerical effect: first-order advection is known to be diffusive, but it is adequate over the period of these simulations.

Fig. 3 (bottom) shows the GW energy density scaled

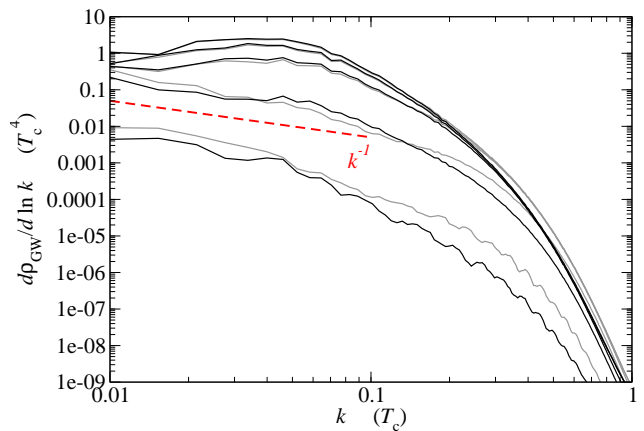


FIG. 4: Gravitational wave power spectra during the phase transition, for the intermediate strength transition, from fluid only (black) and both fluid and field (grey). From bottom to top, the times are $t = 600, 800, 1000, 1200$ and $1400 T_c^{-1}$. The red dotted line indicates the expected k^{-1} behaviour.

by the final value of $(\bar{\epsilon} + \bar{p})^2 \bar{U}_f^{-4}$ and the average bubble size at collision R_* , estimated from $R_*^3 = L^3/N_b$, where N_b is the number of bubbles in the simulation volume. An isolated expanding bubble emits no GWs, which appear only when the bubbles collide. We see that the GW energy density rises linearly after the bubbles have fully merged, sourced by the perturbations in the fluid. The slopes are similar, as expected for a source proportional to $(\bar{\epsilon} + \bar{p}) \bar{U}_f^2$ with scale R_* (see discussion below). Note that the GWs from detonations ($\eta = 0.1$) behave similarly to those from deflagrations.

In Fig. 4 we show the time development of the GW power spectrum as the intermediate strength phase transition proceeds. We see that strong growth happens between $t = 600 T_c^{-1}$ and $t = 1000 T_c^{-1}$ as the bubbles merge (see Fig. 3). For $t \lesssim 1000 T_c^{-1}$ there is evidence of the expected k^{-1} power spectrum, but it becomes less clear as the GW power continues to grow, sourced by the persistent fluid perturbations. At the shortest length scales, we see a v_w -dependent exponential fall-off.

To establish the nature of these fluid perturbations, we show in Fig. 5 the time development of the longitudinal (compressive) and transverse (rotational) components of the fluid velocity power spectrum. At all times, it is clear that most of the fluid velocity is longitudinal, indicating that the perturbations are mostly compression waves. Turbulence generally develops in the transverse components, characterised by a power-law behaviour of the power spectrum. There is some evidence of an almost flat spectrum for $k \lesssim 0.2$, but its significance is unclear.

We can now form a clearer picture of the fluid perturbations and how the GWs are generated. Firstly, we note that the fluid perturbations are initially the form of a compression wave surrounding the growing bubble. The energy in this compression wave grows in proportion

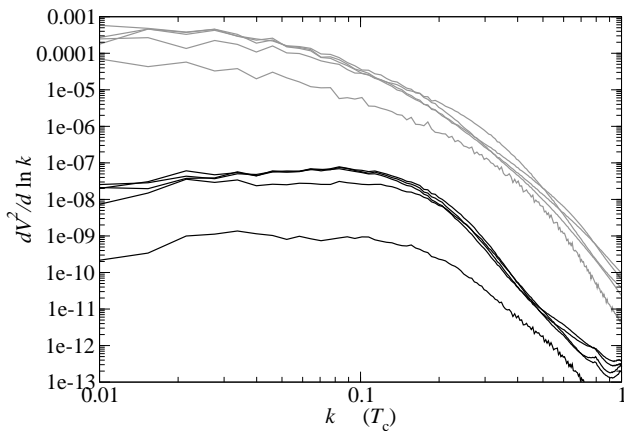


FIG. 5: Fluid velocity power spectra for the intermediate strength transition, separated into longitudinal (compressional) and transverse (rotational) components; shown in grey and black respectively. Times shown are the same as Fig. 4.

to the volume of the bubble R^3 , and quickly outstrips the energy in the scalar field, which grows only as R^2 . The energy in the compression waves remains constant after the bubble merger is complete: as fluid velocities are generally much less than one, their evolution is linear.

The bubble collision generates gravitational waves, as predicted by the envelope approximation, and there is some evidence for the characteristic k^{-1} spectrum between the bubble separation scale R_* and the high-frequency cut-off. The generation of GWs continues long after the merger is completed and the scalar field has relaxed to its new equilibrium value. The GWs are sourced by the compression waves in the fluid. This source of gravitational radiation from a phase transition – sound – has not been appreciated before (except in Ref. [4]).

We can estimate the resulting density of the gravitational waves, in terms of the lifetime of the sound waves τ_s , considered below. The power spectrum is given by

$$\frac{d\rho_{\text{GW}}(k)}{d \ln k} = \frac{2Gk^3}{\pi} \int^t dt_1 dt_2 \cos[k(t_1 - t_2)] \Pi^2(k, t_1, t_2), \quad (11)$$

where $\Pi^2(k, t_1, t_2)$ is the unequal time correlator of the shear stress tensor [28, 36]. We can estimate the amplitude as $[(\bar{\epsilon} + \bar{p})\bar{U}_f^2]^2$, and the length scale as R_* . The coherence time can be written $(c_s k)^{-1} \tilde{\tau}_c(kR_*)$. Hence

$$\Pi^2(k, t_1, t_2) \simeq [(\bar{\epsilon} + \bar{p})\bar{U}_f^2]^2 R_*^3 \tilde{\Pi}^2(kR_*, c_s z / \tilde{\tau}_c), \quad (12)$$

where $z = k(t_1 - t_2)$. The density parameter $\Omega_{\text{GW}} = \rho_{\text{GW}}/\bar{\epsilon}$ is, on using the Friedmann equation,

$$\Omega_{\text{GW}} \simeq \frac{3\bar{\Pi}^2}{4\pi^2} (H_* \tau_s) (H_* R_*) (1+w)^2 \bar{U}_f^4, \quad (13)$$

where H_* is the Hubble parameter at the transition, $w =$

$\bar{p}/\bar{\epsilon} \simeq 1/3$, and

$$\bar{\Pi}^2 = \int d \ln k (kR_*)^2 \int dz \cos(z) \tilde{\Pi}(kR_*, c_s z / \tilde{\tau}_c). \quad (14)$$

In (13) we see the origin of the R_* factor in the GW density, which must be present for dimensional reasons. The slope of the curves in Fig. (3, bottom) is $2\bar{\Pi}^2/\pi$, which we see takes the natural value $\mathcal{O}(1)$, and is weakly dependent on the transition parameters.

The envelope approximation gives [27]

$$\Omega_{\text{GW}} \simeq \frac{0.11 v_w^3}{0.42 + v_w^2} \left(\frac{H_*}{\beta} \right)^2 \frac{\kappa^2 \alpha_T^2}{(\alpha_T + 1)^2} \quad (15)$$

where κ is the efficiency with which latent heat is converted to kinetic energy. Comparing to (13) and noting that $\bar{U}_f^4 \sim \kappa^2 \alpha_T^2$, $R_* \sim v_w/\beta$, we see that sound waves are a more important source by the factor $\tau_s/R_* v_w$.

An upper bound on τ_s is the Hubble time, as the shear stresses decay faster than the background energy density. The shear stresses also decay due to the viscosity η_s , which can be estimated as $\eta_s \sim T^3/e^4 \ln(1/e)$, where e is the electromagnetic gauge coupling [38]. The lifetime of sound waves with characteristic wavelength R_* is therefore $\tau_\eta \simeq R_*^2 \epsilon / \eta_s \sim e^4 \ln(1/e) R_*^2 T_c$. Hence sound waves are the most important source of gravitational waves for bubbles satisfying

$$R_* H_* \gg v_w (\sqrt{a} T_c / m_{\text{Pl}} e^4) \sim 10^{-11} v_w (T_c / 100 \text{ GeV}). \quad (16)$$

This is generally satisfied except for weak transitions at very high temperatures.

We have carried out three dimensional simulations of bubble nucleation, growth and collision during a first order phase transition in the early universe, calculating the resulting gravitational wave power spectrum. We have included a relativistic fluid for the first time. We find that, irrespective of whether it proceeds by deflagration or detonation, the transition creates a background of acoustic waves, which are a more important source of gravitational radiation by the ratio of the fluid damping time τ_s to the duration of the phase transition β^{-1} . For a wide range of parameters, the fluid damping time is the Hubble time, and we conclude that the dominant source of the gravitational wave background from a first order phase transition is the sound it makes.

Our simulations made use of facilities at the Finnish Centre for Scientific Computing CSC, and the COSMOS Consortium supercomputer (within the DiRAC Facility jointly funded by STFC and the Large Facilities Capital Fund of BIS). KR acknowledges support from the Academy of Finland project 1134018; MH and SH from the Science and Technology Facilities Council (grant number ST/J000477/1)

-
- * Electronic address: m.b.hindmarsh@sussex.ac.uk
† Electronic address: s.j.huber@sussex.ac.uk
‡ Electronic address: kari.rummukainen@helsinki.fi
§ Electronic address: david.weir@helsinki.fi
- [1] D. Kirzhnits, JETP Lett. **15**, 529 (1972).
[2] D. Kirzhnits and A. D. Linde, Annals Phys. **101**, 195 (1976).
[3] E. Witten, Phys.Rev. **D30**, 272 (1984).
[4] C. J. Hogan, MNRAS **218**, 629 (1986).
[5] A. Kosowsky, M. S. Turner, and R. Watkins, Phys.Rev. **D45**, 4514 (1992).
[6] A. Kosowsky, M. S. Turner, and R. Watkins, Phys.Rev.Lett. **69**, 2026 (1992).
[7] A. Kosowsky and M. S. Turner, Phys.Rev. **D47**, 4372 (1993), astro-ph/9211004.
[8] M. Kamionkowski, A. Kosowsky, and M. S. Turner, Phys.Rev. **D49**, 2837 (1994), astro-ph/9310044.
[9] K. Kajantie, M. Laine, K. Rummukainen, and M. E. Shaposhnikov, Phys.Rev.Lett. **77**, 2887 (1996), hep-ph/9605288.
[10] M. Laine and K. Rummukainen, Phys.Rev.Lett. **80**, 5259 (1998), hep-ph/9804255.
[11] M. Laine, G. Nardini, and K. Rummukainen, JCAP **1301**, 011 (2013), 1211.7344.
[12] M. S. Carena, M. Quiros, and C. Wagner, Phys.Lett. **B380**, 81 (1996), hep-ph/9603420.
[13] D. Delepine, J. Gerard, R. Gonzalez Felipe, and J. Weyers, Phys.Lett. **B386**, 183 (1996), hep-ph/9604440.
[14] M. Laine and K. Rummukainen, Nucl.Phys. **B535**, 423 (1998), hep-lat/9804019.
[15] C. Grojean, G. Servant, and J. D. Wells, Phys.Rev. **D71**, 036001 (2005), hep-ph/0407019.
[16] S. Huber and M. Schmidt, Nucl.Phys. **B606**, 183 (2001), hep-ph/0003122.
[17] S. J. Huber, T. Konstandin, T. Prokopec, and M. G. Schmidt, Nucl.Phys. **B757**, 172 (2006), hep-ph/0606298.
[18] P. J. Steinhardt, Phys.Rev. **D25**, 2074 (1982).
[19] H. Kurki-Suonio, Nucl.Phys. **B255**, 231 (1985).
[20] K. Kajantie and H. Kurki-Suonio, Phys.Rev. **D34**, 1719 (1986).
[21] K. Enqvist, J. Ignatius, K. Kajantie, and K. Rummukainen, Phys.Rev. **D45**, 3415 (1992).
[22] J. Ignatius, K. Kajantie, H. Kurki-Suonio, and M. Laine, Phys.Rev. **D49**, 3854 (1994), astro-ph/9309059.
[23] H. Kurki-Suonio and M. Laine, Phys.Rev. **D54**, 7163 (1996), hep-ph/9512202.
[24] H. Kurki-Suonio and M. Laine, Phys.Rev.Lett. **77**, 3951 (1996), hep-ph/9607382.
[25] J. R. Espinosa, T. Konstandin, J. M. No, and G. Servant, JCAP **1006**, 028 (2010), 1004.4187.
[26] C. Caprini, R. Durrer, and G. Servant, Phys.Rev. **D77**, 124015 (2008), 0711.2593.
[27] S. J. Huber and T. Konstandin, JCAP **0809**, 022 (2008), 0806.1828.
[28] C. Caprini, R. Durrer, T. Konstandin, and G. Servant, Phys.Rev. **D79**, 083519 (2009), 0901.1661.
[29] H. L. Child and J. Giblin, John T., JCAP **1210**, 001 (2012), 1207.6408.
[30] A. Kosowsky, A. Mack, and T. Kahniashvili, Phys.Rev. **D66**, 024030 (2002), astro-ph/0111483.
[31] G. Gogoberidze, T. Kahniashvili, and A. Kosowsky, Phys.Rev. **D76**, 083002 (2007), 0705.1733.
[32] C. Caprini and R. Durrer, Phys.Rev. **D74**, 063521 (2006), astro-ph/0603476.
[33] C. Caprini, R. Durrer, and G. Servant, JCAP **0912**, 024 (2009), 0909.0622.
[34] J. Garcia-Bellido, D. G. Figueroa, and A. Sastre, Phys.Rev. **D77**, 043517 (2008), 0707.0839.
[35] J. Wilson and G. Matthews, Relativistic Numerical Hydrodynamics (Cambridge University Press, Cambridge, 2003).
[36] D. G. Figueroa, M. Hindmarsh, and J. Urrestilla, Phys. Rev. Lett. **110**, **101302** (2013), 1212.5458.
[37] N. Bevis, M. Hindmarsh, M. Kunz, and J. Urrestilla, Phys.Rev. **D82**, 065004 (2010), 1005.2663.
[38] P. B. Arnold, G. D. Moore, and L. G. Yaffe, JHEP **0011**, 001 (2000), hep-ph/0010177.